Unidirectional spin-torque driven magnetization dynamics

Joseph Sklenar, Wei Zhang, Matthias B. Jungfleisch, Hilal Saglam, Scott Grudichak,
Wanjun Jiang, John E. Pearson, John B. Ketterson, and Axel Hoffmann

Unidirectional spin-torque driven magnetization dynamics

Joseph Sklenar,[1,2,*] Wei Zhang,[1,3] Matthias B. Jungfleisch,[1] Hilal Saglam,[1,4] Scott Grudichak,[2] Wanjun Jiang,[1,5,6] John E. Pearson,[1] John B. Ketterson,[2] and Axel Hoffmann[1]

[1]*Materials Science Division, Argonne National Laboratory, Lemont IL 60439, USA*
[2]*Department of Physics and Astronomy, Northwestern University, Evanston IL 60208, USA*
[3]*Department of Physics, Oakland University, Rochester MI 48309, USA*
[4]*Department of Physics, Illinois Institute of Technology, Chicago IL 60616, USA*
[5]*State Key Laboratory of Low-Dimensional Quantum Physics and Department of Physics, Tsinghua University, Beijing 100084, China*
[6]*Collaborative Innovation Center of Quantum Matter, Beijing 100084, China*
(Dated: May 3, 2017)

The rich physics associated with magnetism often centers around directional effects. Here we demonstrate how spin-transfer torques in general result in unidirectional ferromagnetic resonance dynamics upon field reversal. The unidirectionality is a direct consequence of both field-like and damping-like dynamic torques simultaneously driving the motion. This directional effect arises from the field-like torque being odd and the damping-like torque being even under field reversal. The directional effect is observed when the magnetization has both an in-plane and out-of-plane component, since then the linear combination of the torques rotates with a different handedness around the magnetization as the magnetization is tipped out-of-plane. The effect is experimentally investigated via spin-torque ferromagnetic resonance measurements with the field applied at arbitrary directions away from the interface normal. The measured asymmetry of the voltage spectra are well explained within a phenomenological torque model.

I. INTRODUCTION

Spin-transfer-torques are key to fundamental and applied advances in the field of spintronics[1]. Spin-transfer torques occur when a non-equilibrium spin accumulation (typically generated by an electric curent) interacts with the magnetization of a ferromagnet[2–5]. These interactions can lead to two different torques acting on the magnetization, which due to their distinctive symmetries are known as field-like (FL) and (anti) damping-like (DL) torques. The FL torque is odd with respect to a global reversal of the magnetization, while the DL torque is even. Thus, the possibility of a unidirectional response in spin-torque driven magnetization dynamics (the precessional motion) with respect to field reversal is expected. Yet there have been no reports of a dynamic unidirectionality in the time since spin-torque ferromagnetic resonance was first measured in spin valves[6,7] and in permalloy(Py)/Pt (FM/NM) bilayers which were first measured by Liu *et al.*[8]. We show that to induce unidirectional dynamics the applied magnetic field must have both an in-plane and out-of-plane component; these field configurations are typically not explored in spin torque ferromagnetic resonance (ST-FMR) measurements.

Originally, spin-transfer torques (STT) were investigated in nano-contacts and nanopillars[10,11]. More recently, simplified planar structures utilizing the spin Hall effect as a spin current source have been appearing[8]. The material systems studied include spin Hall metals[12,13], topological insulators[14], antiferromagnets[15], two-dimensional interfaces including both transition metal dichalcogenides and metallic interfaces[16,17], and magnetic insulators[18–22]. It is worth noting that the dynamic unidirectionality we report appears in the same system where other independent unidirectional magnetic phenomena have been found. In particular, a new type of unidirectional magnetoresistance has been observed in Pt/Co and Ta/Co (FM/NM) systems where the unidirectionality comes from two different resistances for majority and minority spins at the FM/NM interface[23]. Another independent example of unidirectionality has been the demonstration of the Dzyaloshinskii-Moriya interaction in FM/NM systems leading to a linear term in spin wave dispersion relationships[24,25].

The FM/NM films studied here will be "arbitrarily magnetized": i.e., by tipping the magnetization out-of-plane (OOP) the magnetization will have both in-plane and OOP components. For arbitrary configurations, we find that the ST-FMR signal no longer has mirror symmetry under magnetic field reversal. The asymmetry is a consequence of the time varying DL and FL torque simultaneously acting on the FM. By solving for the linear FMR response we show that when both DL and FL torques drive the magnetization, an arbitrarily magnetized slab will have an asymmetric response. This originates from an asymmetry in how the linear combination of FL and DL torques rotate around the magnetization. This result should have implications for STT switching , a central issue in spintronics[30]. Additionally, we developed a model to measure the ratio of the DL-to-FL torques (τ_D/τ_F) as a function of the OOP angle. We find that as the magnetization is tipped OOP, τ_D/τ_F changes. First and second harmonic anisotropic magnetoresistance and Hall measurement of similar heterostructures[26–29] previously indicated an out-of-plane angular dependence of τ_D and τ_F. However, our work indicates that the change in τ_D/τ_F is also asymmetric with respect to magnetic field reversal.

II. EXPERIMENTAL DESIGN AND TORQUE PHENOMENOLOGY

In ST-FMR experiments the magnetic layer is described as a single macrospin given by the unit vector $\hat{\mathbf{m}}$. The equation of motion governing this macrospin is the Landau-Lifshitz-
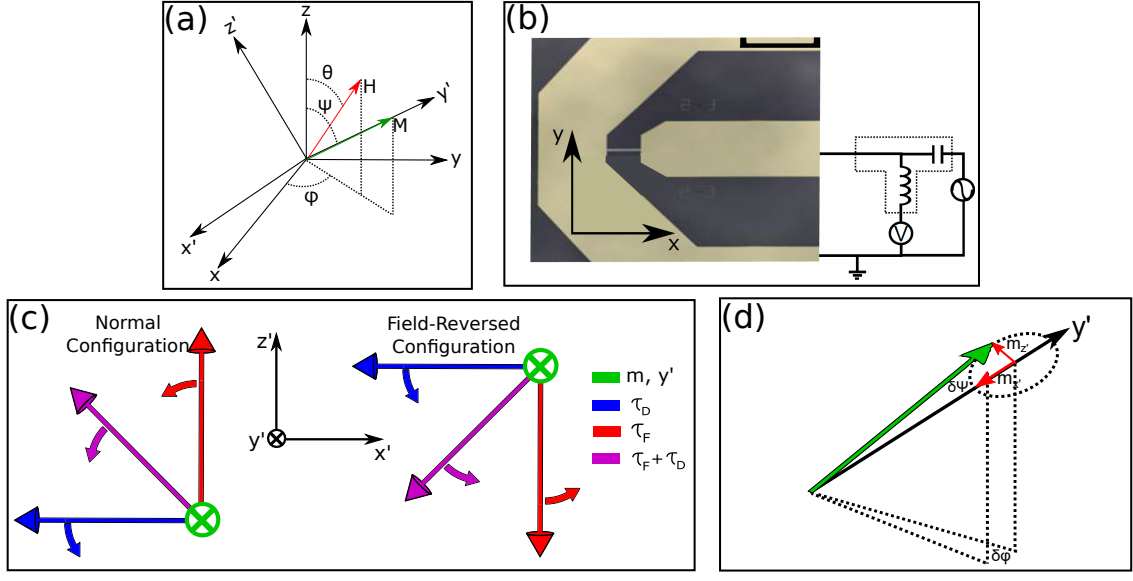
FIG. 1. (a) The coordinate system describing the field and magnetization. (b) ST-FMR measurement geometry: a narrow Py/Pt bilayer bar spans the gap (along x-axis) between the central line and the two return ground lines of a co-planar waveguide. In (c) we plot the magnetization and FL and DL torques for two magnetization configurations that are reversed with respect to each other. The magnetization is always assumed to lie in the y' direction and the FL and DL torques lie in the x'z' plane. The colored arrows represent individual FL (red) and DL (blue) torques and the combination of a FL and DL torque (purple). There is an asymmetry in the rotation direction for the linear combination of FL and DL torques. In the normal configuration, where θ is between 0°-90° the torque combination will rotate towards the original DL torque orientation. For the field-reversed configuration the torque combination will rotate towards where the FL torque orientation. (d) Dynamic magnetization amplitudes for the magnetization precessing around the y' axis are related to differential changes in the angles.
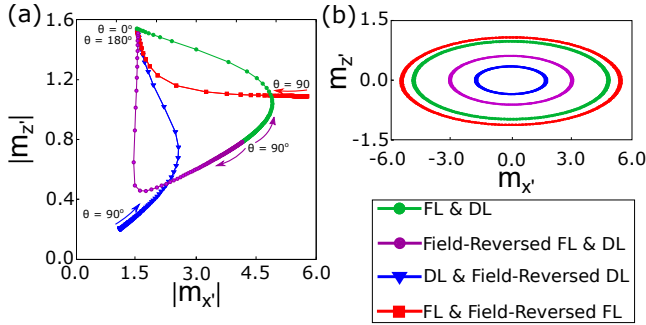

FIG. 2. (a) Trajectories of the magnitudes of (m'_x, m'_z) for $\phi = 45°$ [225° for field reversed (FR)], where each data point is a different (θ, ψ) pair. Each curve starts at $\theta = 90°$ (indicated by arrows) and ends at $\theta = 0°$ or $\theta = 180°$. Each point is derived from static equilibrium considerations. The red curve corresponds to the pure FL case while the blue curve is the pure DL case. The red and blue curves each represent the case where θ varies from $90° \to 0°$ and $90° \to 180°$. The green curve is the mixed torque case where $\tau_D = \tau_F$; here θ varies from $90° \to 0°$. The purple curve is the FR case where $90° \to 180°$ and again both torques are present. In (b) we plot the elliptical FMR trajectories of (m'_x, m'_z) at $(\phi, \theta, \psi) = (45°, 8°, 75°)$ and $(225°, 172°, 105°)$ for the FR case. When both torques are present the FMR trajectory is not invariant with respect to FR.

Gilbert equation:

$$\frac{d\hat{\mathbf{m}}}{dt} = -\gamma\hat{\mathbf{m}}\times\mathbf{H}_{eff}+\alpha\hat{\mathbf{m}}\times\frac{d\hat{\mathbf{m}}}{dt}+\gamma\tau_F\hat{\mathbf{m}}\times\hat{y}+\gamma\tau_D\hat{\mathbf{m}}\times(\hat{y}\times\hat{\mathbf{m}}). \quad (1)$$

In Eq. (1) γ is the gyromagnetic ratio, $\mathbf{H}_{eff}$ is the effective magnetic field, and α is the damping parameter. There are two torque terms that oscillate at the microwave frequency, τ_F and τ_D. These torques originate from an oscillating Oersted field in the y-direction, and an oscillating spin current passing into the Py from the Pt, polarized along y. The directions are given by the device geometry, and the spin current originates from the spin Hall effect in Pt[1,9]. Figs. 1 (a) and (b) show the coordinate system and sample. The magnetization is described by the in-plane azimuthal angle ϕ and the polar angle ψ. The applied magnetic field $\mathbf{H}$ is described by the same angle ϕ and the polar angle θ. We can solve Eq. (1) for the arbitrarily magnetized case using a coordinate system that is rotated such that the magnetization points along one of the axes; this is the (x'y'z') system drawn in Fig. 1 (a). In Fig. 1 (c), the unidirectional response in the dynamics of the Py/Pt bilayer is illustrated. The three vectors $\hat{\mathbf{m}}$, $\tau_F = [\hat{\mathbf{m}}\times\hat{y}]$, and $\tau_D = \hat{\mathbf{m}} \times (\hat{y} \times \hat{\mathbf{m}})$ are not all even or odd under field reversal. As the magnetization is rotated OOP the linear combination of $\tau_F + \tau_D$ will tend to rotate towards the original FL torque orientation for the normal configuration, and for the field-reversed situation $\tau_F + \tau_D$ rotates towards the original DL torque orientation.

We are interested in the dynamic amplitudes (m'_x, m'_z) as a function of (ϕ, θ, ψ). These quantities, shown in Fig. 1 (d), are asymmetric with respect to magnetic field reversal (see Supplemental). Here we define field reversal (FR) as $H(\phi, \theta) \to H(\phi + 180°, 180° - \theta)$. In Fig. 2 (a) we plot the dependence of the magnitude of m'_x and m'_z as a function of
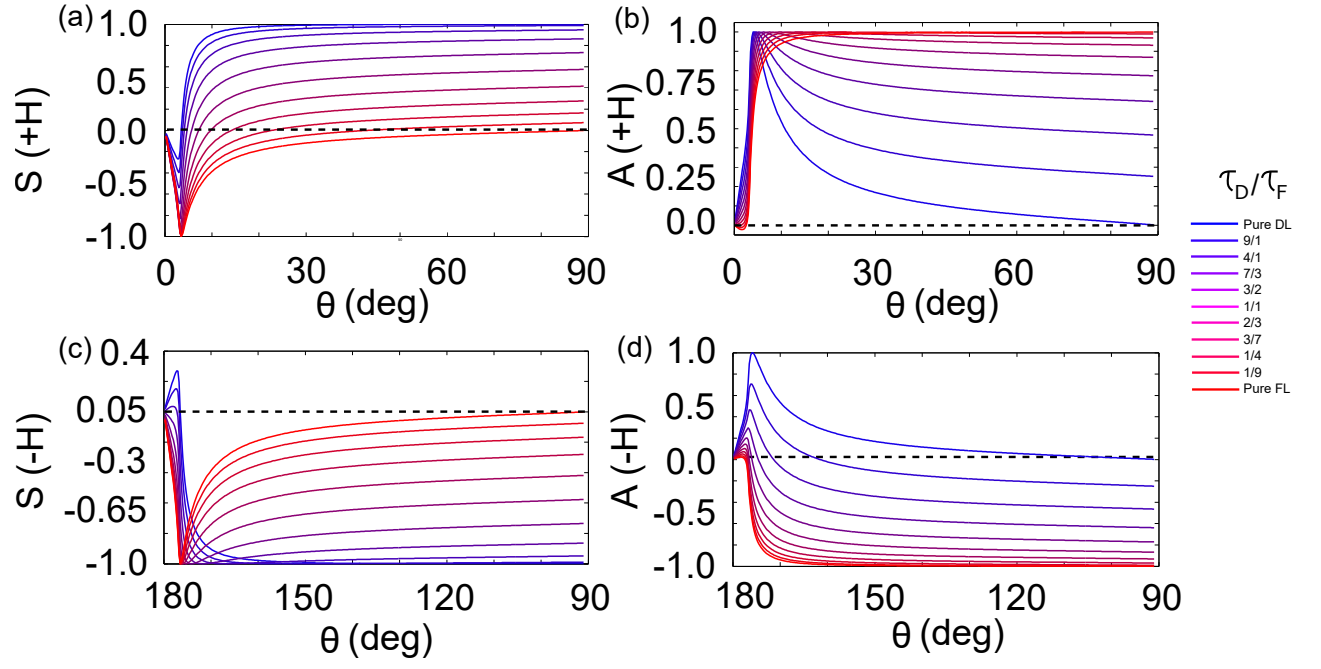
FIG. 3. The results of combining the phenomenological torque model with AMR rectification are presented here. We plot the coefficients 'S' and 'A' for '+' fields as well as FR '-' configurations as a function of θ for various ratios of τ_D/τ_F. For a pure damping-like or a pure field-like torque the angular dependence will either be symmetric or mirror-symmetric under field reversal for both 'A' and 'S'. A combination of each has no such symmetry when the magnetic field is reversed as a function of θ. The strongest prediction of our model is that the symmetric amplitude 'S' will change sign for '+' fields as θ is decreased but will remain the same for negative fields. Similarly the antisymmetric amplitude 'A' will change sign for '-' fields but will remain the same for '+' fields. This qualitative prediction is observed in our experimental data in Fig. 4.

θ for the normal and FR case. In Fig. 2 (a) trajectories are drawn for m'_x and m'_z for the pure FL case in red, and the pure DL case in blue. Each data point represents a different value for the angles θ and ψ. The trajectories all start at $\theta = 90°$ (in-plane) and end at a circular orbit when the field is OOP ($\theta = 0°, 180°$). For the pure FL and DL torque cases these trajectories are invariant with respect to FR. On the other hand, a strong asymmetry is observed for the situation where both torques are present ($\tau_F = \tau_D$). The green and purple circles represent the normal and the FR case, respectively. In Fig. 2 (b) we plot the precessional motion in the x'z' plane for (θ, ψ) = (8°, 75°) and (θ, ψ) = (172°, 105°). Again, the red and blue trajectories represent pure field and damping-like torques that are invariant under FR. The green curve represents the normal case where $\tau_F = \tau_D$, and the purple curve represents the FR configuration. The elliptical precessional motion has a notably larger cone angle for the normal case compared to the FR case offering a picture of dynamic unidirectionality.

The unidirectional dynamics are detected by a rectification related to anisotropic magnetoresistance (AMR)[31]. At FMR a dc voltage is generated across the ferromagnet due to mixing of oscillating AMR with microwaves passing through the sample[32–38]. The amplitude of the dynamic AMR, δR, can be expressed in terms of two angular amplitudes $\delta\phi$ and $\delta\psi$ [Fig. 1 (c)] that describe the precession:

$$\delta R = \frac{\partial R}{\partial \phi}\delta\phi + \frac{\partial R}{\partial \psi}\delta\psi, \tag{2}$$

and the angular amplitudes are related to the magnetization amplitudes as $\delta\phi = m_{x'}$ and $\delta\psi = m'_z$. The dc voltage that develops across the sample near and on resonance is given as $V_{dc} = \frac{1}{2}I_{rf}\delta R$, where I_{rf} is the microwave current passing through the FM. It can be shown (see Supplemental) that the measured lineshape can be decomposed into a symmetric and antisymmetric part:

$$V_{dc} = \frac{S\Delta + A(\omega^2 - \omega_0^2)}{(\omega^2 - \omega_0^2)^2 + \Delta^2}. \tag{3}$$

The amplitudes S and A are listed below in Eqs. (4) and (5). They contain a non-trivial angular dependence, and measured ratios of S/A can yield the ratio of damping to field-like torque without measuring the quantity I_{rf}. The quantity Δ is the linewidth parameter. For a variety of torque ratios the OOP angular dependence of Eqs. (4) and (5) are plotted in Fig. 3.

$$S = \frac{1}{2}I_{rf}[\frac{\partial R}{\partial \phi}\omega\gamma(\tau_D\cos\psi\sin\phi + \tau_F\cos\phi)-$$
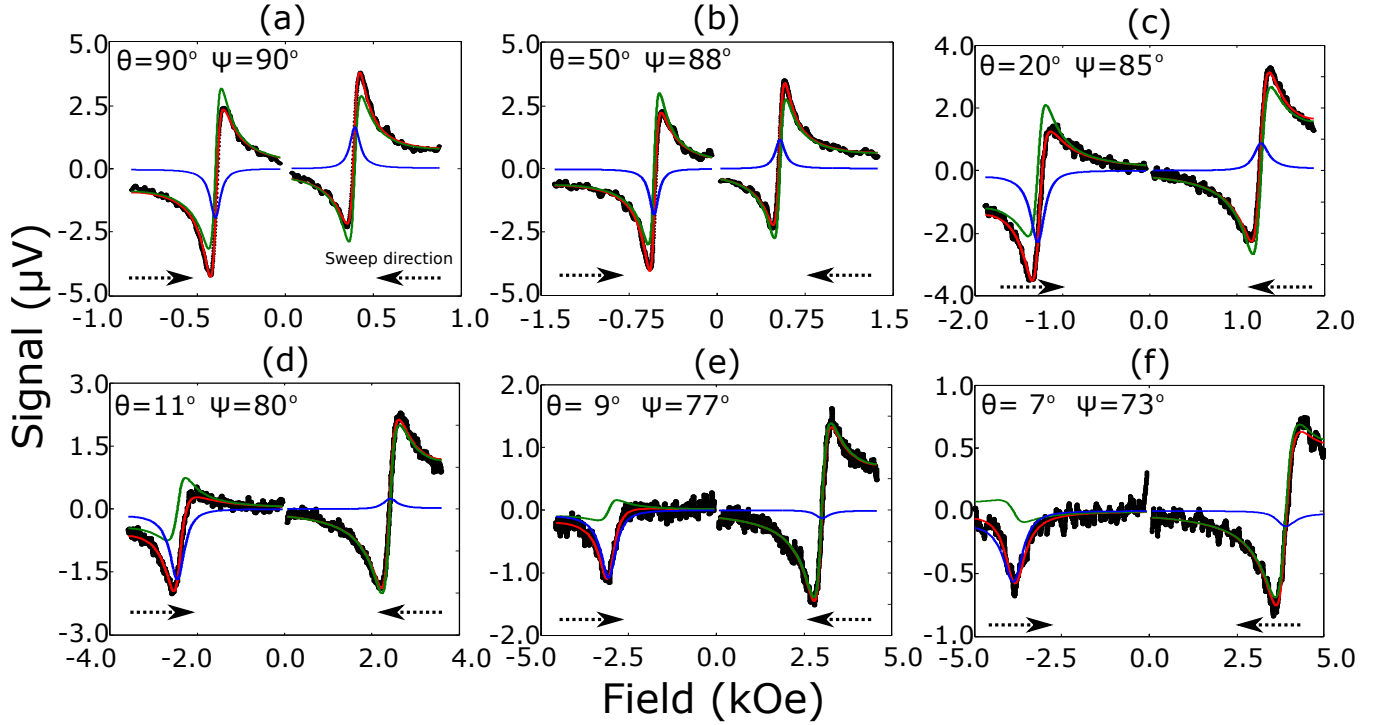$$\sin\psi\frac{\partial R}{\partial \psi}\omega\gamma(\tau_D\cos\psi\sin\phi + \tau_F\cos\phi)] \tag{4}$$

FIG. 4. Experimental ST-FMR signals for field configurations with $\phi = 45°$ (225° for FR) are shown. (a)-(d) show the ST-FMR signal as a function of field and each plot contains both the '+' and '-' field reversed responses. The '-' fields are the FR case. Black curves are data while red curves are the fit obtained from Eq. (3). The blue and green curves are the two terms in Eq. (3) that are proportional to 'S' and 'A' respectively. As the field is tipped OOP the ST-FMR signal loses mirror symmetry under FR. The fields where the resonances occur are in agreement with the Kittel equation for the uniform mode (see Sec. IV).

$$A = \frac{1}{2}I_{rf}[\frac{\partial R}{\partial \phi}\gamma^2(\tau_D \cos \psi \sin \phi + \tau_F \cos \phi)\times$$

$$(H_0 \cos (\theta - \psi) - 4\pi M_{eff} \cos 2\psi) - \sin \psi \frac{\partial R}{\partial \psi}\gamma^2(\tau \cos \phi -$$

$$\tau_F \sin \phi \cos \psi)(H_0 \cos (\theta - \psi) - 4\pi M_{eff} \cos \psi^2)] \quad (5)$$

One can note that the red and blue curves in Fig. 3 represent a pure FL and DL torque respectively. When comparing S(+H) to S(-H) and A(+H) to A(-H) for the red and blue curves they will either be mirror images or unchanged upon field-reversal. Any of the other curves which represents a combination of a FL and DL torque does not have the property that upon field-reversal it is invariant or a mirror-image of itself. This is a manifestation of the dynamic unidirectionality in the line-shape.

III. OUT-OF-PLANE ST-FMR EXPERIMENTAL RESULTS

To perform ST-FMR experiments the configuration shown in Fig. 1 (b) is used where a Py/Pt bar shorts a Ti/Au co-planar waveguide (CPW). The Py/Pt bilayer is 90×20 μm^2 in area with 5-nm thick Py and 10-nm thick Pt. A bias-tee configuration facilitates simultaneously passing microwaves through the sample while monitoring the dc voltage. We fixed the experimental microwave frequency at 5.5 GHz with 10 dBm of power and amplitude modulated the microwaves at 4 kHz for

lock-in detection of the dc voltage. We verified that our sample was producing the appropriate FL and DL torques in Eq. (1) by varying the in-plane angle ϕ (see Sec. IV) at $\theta, \psi = 90°$. Next, the angle ϕ was fixed at 45° and θ was varied from 90° - 7°. For every value of θ we also collected data with the field reversed such that $\theta \rightarrow 180° - \theta$, $\psi \rightarrow 180° - \psi$ and $\phi \rightarrow 225°$. Fig. 4 shows six representative ST-FMR traces in the normal configuration accompanied by their FR counterparts plotted as negative field values. In Fig. 4 (a), $\theta = 90°$ and the field lies in the sample plane; thus, reversing the magnetic field only changes the azimuthal angle ϕ and the ST-FMR signal is mirror symmetric. In Fig. 4 (b) and (c) $\theta = 50°$ and $\theta = 20°$. Although a large range of angles is covered here only a subtle asymmetry in the ST-FMR signal under FR is observed. Specifically, there is a slight reduction in the symmetric amplitude relative to the antisymmetric amplitude for the '+' fields while for the '-' fields the antisymmetric amplitude is reduced relative to the symmetric amplitude. In Fig. 4 (d)-(f) $\theta = 11°$, 9°, and 7°. In this angular range the unidirectionality from the combination of the FL torque and the DL torque presents itself unambiguously. For $\theta = 11°$ (Fig. 4 (b)) the symmetric amplitude is heavily suppressed compared to its FR counterpart at $\theta = 169°$. Likewise the antisymmetric component at $\theta = 169°$ is suppressed compared to $\theta = 11°$. In Fig. 4 (c), the symmetric amplitude for the positive field startlingly changes signs. Here for both $\theta = 9°$ and $\theta = 171°$ the sign of the symmetric amplitude is negative. In Fig. 4
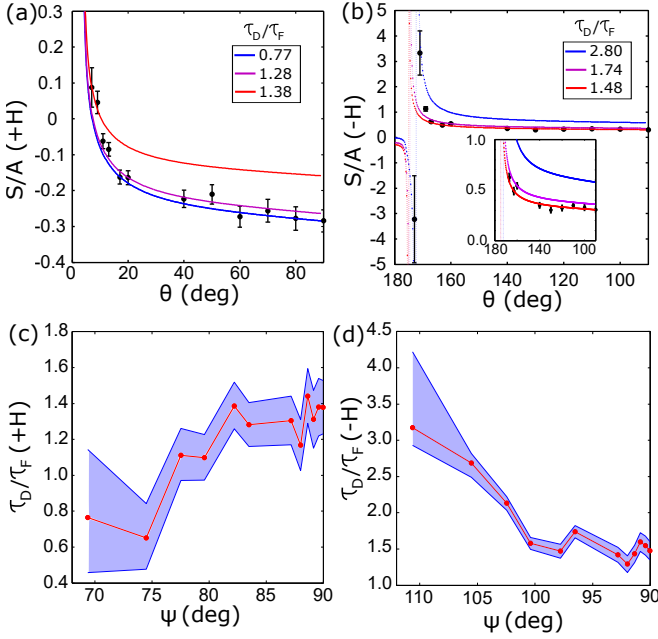
FIG. 5. We plot the experimental amplitude ratio, S/A, as a function of θ and compare with theory. In (a) we consider the '+' fields and find that a ratio of τ_D/τ_F = 1.48 well describes a large part of the angular range but as the magnetization is tipped out of plane, curves with *decreasing* ratios better intersect the data points. For '-' orientations (b) when θ is small the ratio of τ_D/τ_F needs to *increase* in order to intersect the data points. In (c) and (d) we allow for the ratio of τ_D/τ_F to be a free parameter for '+' fields and '-' fields respectively. There is an asymmetry in the trend of τ_D/τ_F; the '+' configuration suppresses the ratio as the magnetization is tipped OOP while the '-' configuration increases the ratio.

(d) the asymmetric component of ST-FMR lineshape changes signs for negative fields (θ = 173°). At this orientation, for θ = 7° and θ = 173°, the unidirectional ST-FMR signal is strongest. The sign changes in both the antisymmetric and symmetric amplitude are predicted by Eqs. (4) and (5).

The torque model we use to analyze our data combines Eqs. (3)-(5). The blue and green curves in Fig. 4 show a plot of S and A for each ST-FMR curve from which we can extract τ_D/τ_F as a function of θ. In Fig. 5 (a) and (b) we plot S/A as a function of θ for the normal case and FR case. The theoretical curves for a ratio of τ_D/τ_F near 1.5 describe many angles, but as the field is tipped out-of-plane other torque ratios match the data better. The inset in Fig. 5 (b) shows the behavior for small tipping angles for the ratio. In Fig. 5 (c) and (d) we allow the torque ratio to change to best fit each data point in (a) and (b). For the normal configuration τ_D/τ_F decreases to values closer to 0.6 while for the FR configuration there is an increase to values closer to 3.0. We strongly emphasize that this torque asymmetry is independent of the intrinsic unidirectionality in the precession of the magnetization. It forces us to conclude that the polarity of the applied magnetic field influences the OOP angular dependence of τ_D/τ_F, or that there is an unaccounted for asymmetric rectification mechanism. We should compare the OOP result with the second harmonic measure-

ment technique that previously measured field reversal symmetric DL and FL torques in the OOP geometry[27]. These measurements were done in Co/Pt cross structures and it is unclear if the qualitative discrepancy in our result is due to materials, metrology, or a new rectification mechanism in ST-FMR. The OOP angular dependence of the DL to FL torque does is similar to a previous result we obtained for ST-FMR in YIG/Pt. In this work we found that the real and imaginary parts of the spin mixing conductance varied as a function of θ and ψ[21]. Currently, the model used to understand the YIG/Pt system has a more complicated set of parameters together with an rectification mechanism, thereby making a direct comparison of the present work (Py/Pt) to YIG/Pt difficult.

IV. DETERMINING SPIN-TORQUES FROM THE IN-PLANE ST-FMR ANGULAR DEPENDENCE

Lineshape analysis has previously been problematic in interpreting related experiments. A prominent example was pointed out by Harder *et al.* where it was shown that for certain experimental device designs large phase shifts between the Oersted field and the microwave current could occur in a narrow frequency range[39]. In that work, an essentially symmetric lineshape was transformed to an antisymmetric one in a 500 MHz interval. Previous ST-FMR measurements in Py/Pt show no strong evidence for a phase shift[8,40] and and the same applies to the measurements reported here (see Appendix). Regardless, the experiment by Harder implies lineshape analyses should be performed with care.

It is important to measure the in-plane, ϕ, dependence of the ST-FMR lineshape prior to measuring the θ dependence since it can be used to rule out additional unwanted torques acting on the system; this point has been independently demonstrated by Skinner[41]. As an example, poor sample design can produce apparent FL or DL torques in the x-direction or z-direction. The presence of such torques would complicate an OOP angular study which assumes a single FL and DL torque in the y-direction, and would require additional fitting parameters. One of the attractive features of the analysis we performed on the OOP ST-FMR dataset was that it involved only the single fitting parameter τ_D/τ_F. In a separate work we tabulated the in-plane angular dependence of the symmetric and antisymmetric component of the lineshapes based on different phenomenological torques[42].

For our material system and chosen coordinates, the two torques that we expect arise from a field in the y-direction and a spin accumulation in the y-direction. The resulting FL and DL torques should have a $\cos\phi\sin 2\phi$ angular dependence for both the antisymmetric and symmetric component of the lineshape, where the $\sin 2\phi$ component comes from the derivative of the AMR, which has a $\cos(\phi)^2$ behavior. In addition to the CPW geometry that was shown in Fig. 1 (b), we used an alternate geometry in which a rectangular Py/Pt bar shorted two square contact pads and where the bar had dimensions of 100 × 500 μm^2 with Pt and Py thicknesses of 5 nm and 10 nm respectively.

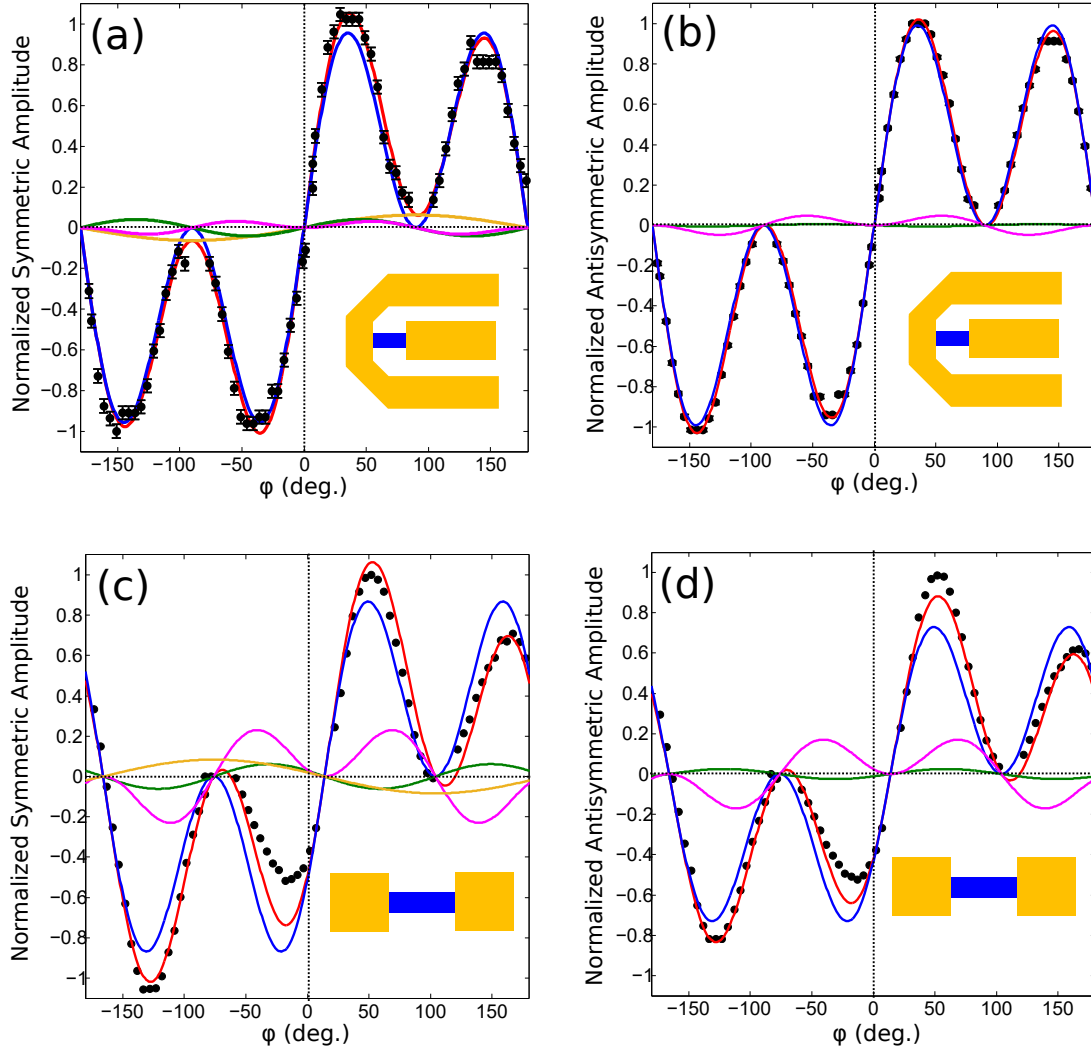In Fig. 6 (a) and (b) we plot the in-plane angular depen-

FIG. 6. The in-plane ST-FMR angular dependence of both the symmetric and antisymmetric components of the lineshape are shown above. Two device geometries are considered. In (a) and (b) the symmetric and antisymmetric components for the CPW are shown. The CPW device is the same device in which the OOP ST-FMR measurements were made on. In (c) and (d) the same lineshape components are shown for a different device geometry. In this other geometry a Py/Pt rectangular bar shorts two contact Ti/Au contact pads. An extensive description of this data is provided in the text. For a quick reference, the black data points are fit to a cumulative signal which is the red curve. For the symmetric component of the lineshape the blue curve is phenomenolgically related to a DL torque in the y-direction, the pink curve is related to a FL torque in the x-direction, the green curve a FL torque in the z-direction, and the gold curve is a sinusoidal spin pumping curve. For the antisymmetric component the blue curve is related to a FL torque in the y-direction, the pink curve is a DL torque in the x-direction, and the green curve is related to a DL torque in the z-direction.

dence of the symmetric and antisymmetric components of the lineshape respectively for the same CPW sample used for the OOP ST-FMR measurements. For the symmetric component (a) the total fit is shown as a red line which is a summation of four terms: $\cos\phi\sin 2\phi$ (blue), $\sin\phi\sin 2\phi$ (pink), $\sin 2\phi$ (green), and $\sin\phi$ (gold) term. A $\sin\phi\sin 2\phi$ suggests a DL torque in the x-direction and a $\sin 2\phi$ behavior is indicative of a FL torque in the z-direction. Finally, for the symmetric amplitude we include a $\sin\phi$ term to account for any potential spin pumping effects[21]. As expected, the blue curve dominates the cumulative fit, which is consistent with a DL torque in the y-direction; this is exactly what we expect for our geometry. If we take the amplitude ratio of the $\sin\phi$ component

of the fit, relative to the expected $\sin\phi\sin 2\phi$ behavior, we find that there may be a spin pumping signal at the 5% level. Contributions to the symmetric signal from a DL torque in the x-direction or a FL torque along the z-direction are no greater than 3%. Similarly, for the antisymmetric lineshape shown in (b), the total fit (red) is dominated by a $\cos\phi\sin 2\phi$ (blue) curve which is expected for a FL torque in the y-direction. We do allow the total fit to have a $\sin\phi\sin 2\phi$ (pink) and a $\sin 2\phi$ (green) contribution which would arise from a FL torque in the x-direction and a DL torque in the z-direction respectively. We find that there is no more than a 5% contribution from a FL torque in the x-direction and that any DL torque in the z-direction is at a level of less than 1%.

Fig. 6 (c) and (d) show the in-plane ϕ dependence of the symmetric and antisymmetric amplitude for the shorted rectangle device. The color scheme is identical to that used for (a) and (b). For this device it is immediately clear that there is a larger contribution to the angular dependence from terms others than $\cos\phi\sin 2\phi$. For the symmetric amplitude the $\sin\phi\sin 2\phi$ (pink) contribution is about 25% of the main $\cos\phi\sin 2\phi$ signal, which suggests a sizable DL torque in the x-direction. The green and gold curves are both at roughly the 5% level, implying contributions from OOP FL torque and spin pumping. There is a peculiarity with the potential spin pumping signal. The $\sin\phi$ signal has the opposite polarity of that which is expected relative to the CPW sample. Clearly, there are unwanted torques present for this geometry and the phenomenological torque model is seemingly not able to fit the data in (c) to the same degree as in (a). In Fig. 6 (d) the antisymmetric angular dependence for the shorted rectangle also shows a departure from what is expected. Specifically, there is an apparent contribution from a FL torque in the x-direction, again at the 25% level, as evidenced by the pink curve. There is also a DL torque in the z-direction at roughly the 5% level illustrated by the green curve. For the shorted rectangular bar device the presence of sizable FL and DL torques in the x-direction seems inescapable. An OOP ST-FMR lineshape analysis of this dataset would require a more complicated phenomenological model which we did not pursue. We note that this dataset should serve as a warning; without a full angular in-plane dataset unanticipated torques cannot be fully identified. Any analysis of data in a limited angular range that makes assumptions about the torques present could then lead to inaccurate extracted torque values. Even in a system as well-studied as Py/Pt, it is apparent that different sample designs cause departures from the expected behavior.

V. CONCLUSIONS

In conclusion, we have demonstrated that unidirectionality appears in the ST-FMR signal for arbitrarily magnetized magnetic films that are simultaneously under the influence of a damping-like torque and field-like torque. This is due to a dynamic unidirectional magnetization effect which is related to the symmetry of the driving torques under magnetic field reversal. The dynamics are detected through an AMR rectification effect which we model. An unexpected result of our experiment is the apparent dependence of τ_D/τ_F on θ and ψ and it's asymmetry under magnetic field reversal. Looking forward, the asymmetric angular dependence of τ_D/τ_F may possibly arise from a precession of the electrically generated spin accumulation around the applied magnetic field direction giving rise to spin accumulations along the x- and z-axis. Such a precession may give rise to additional FL and DL contributions that are not taken into account by our model. Within the confines of our model this may result in an asymmetric torque effect. We also point out that a comprehensive in-plane angular study of the ST-FMR lineshape is essential in determining which phenomenological torques are present. This is especially important when analyzing the more complicated angular dependence of the out-of-plane ST-FMR signal.

VI. APPENDIX

A. Ferromagnetic resonance in arbitrarily magnetized films

For the case of an in-plane magnetized, isotropic ferromagnetic film it is well known that the resonant excitation of the uniform mode can be described by the Kittel equation. The Kittel equation is:

$$\omega_0 = \gamma\sqrt{H_0(H_0 + 4\pi M_{eff})}, \tag{6}$$

where γ is the gyromagnetic ratio, H_0 is the applied magnetic field, and M_{eff} is the effective saturation magnetization. Ferromagnetic resonance can take place for an arbitrarily magnetized slab as well. To describe an arbitrarily magnetized ferromagnetic slab we will require the two polar angles, θ and ψ, defined in the main body of the text, that describe the applied field and magnetization respectively. Due to geometric demagnetization it is generally not the case that θ and ψ are the same. The relation between the two angles can be found from the condition of static equilibrium, $\hat{\mathbf{m}}\times\mathbf{H_{eff}} = 0$. Here $\mathbf{H_{eff}}$ includes the static demagnetization field from the finite thickness of the film and $\mathbf{H_{eff}} = \mathbf{H_0} - 4\pi M_{eff}\cos\psi\hat{\mathbf{z}}$. Thus, the static equilibrium condition can be expressed as:

$$\cos\psi\sin\psi + \frac{H_0}{4\pi M_{eff}}(\cos\psi\sin\theta - \sin\psi\cos\theta) = 0. \tag{7}$$

The modified Kittel equation can be obtained from solving the LLG equation of motion and it is found that

$$\omega_0^2 = \gamma H_0^2 + H_0 4\pi M_{eff}(\sin\theta\sin\psi - 2\cos\theta\cos\psi) + (4\pi M_s)^2\cos^2\psi. \tag{8}$$

By numerically solving for ψ (for a given θ) in Eq. (7), the resulting (θ, ψ) pair can be subsituted into Eq. (8) to either solve for the resonance field at a fixed frequency or vice-versa. Because we fixed ω in our experiment we are interested in solving for the resonant field at various values of θ and ψ. Furthermore we need to consider how ψ will vary for a fixed
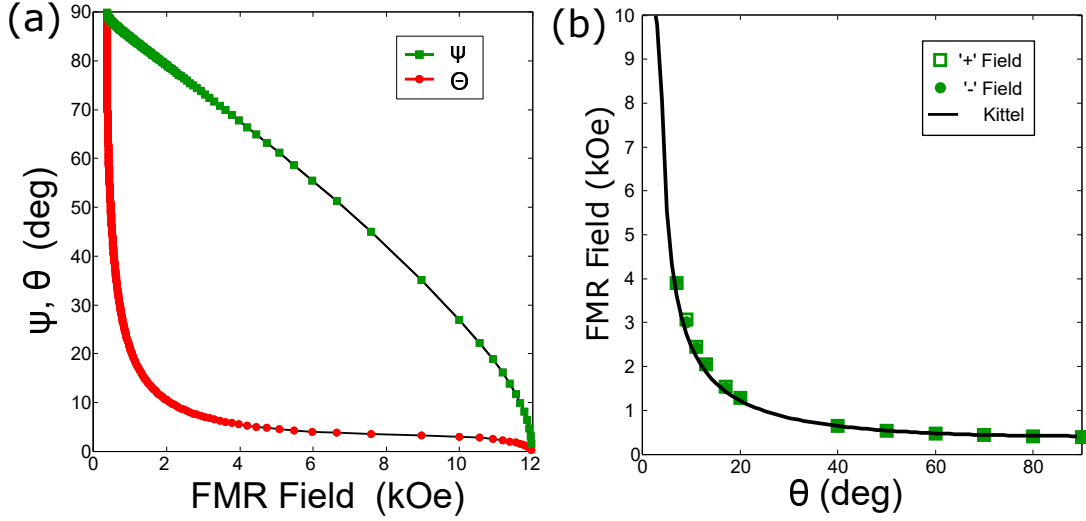
FIG. 7. In (a) we plot the configuration of θ and ψ as a function of the FMR resonant field when the frequency is fixed at 5.5 GHz. We employ these results in our phenomenological model used in the main text. In (b) we plot the FMR resonance field position for both '+' and '-' fields as a function of θ and fit to the Kittel equation. The magnitude of the resonant field is independent of field orientation which suggests that we are measuring a non-hysteretic, uniform FMR excitation.

θ within the vicinity of the resonant field. In Fig. 7 (a) we plot the resonant field as a function of both θ and ψ to show the difference between these two angles at various arbitrarily magnetized configurations. The frequency is fixed at 5.5 GHz for this plot, consistent with the experiment. In Fig. 7 (b) we plot the resonant field of the FMR mode that we discuss in the main paper as a function of θ. The green open squares correspond to the positive field values while the green filled circles correspond to the negative field values when the field is reversed such that $\theta \rightarrow 180° - \theta$, $\psi \rightarrow 180° - \psi$. The black line is the Kittel fit from Eq. (8). From the agreement of the fit with both types of data points, we conclude that there are no hysteresis effects and that both field configurations are adequately described by a uniform mode excitation. The only free parameter throughout this fitting procedure is M_{eff} and we find that $4\pi M_{eff}$ is roughly 9.1 kG from this analysis.

B.   Anisotropic magnetoresistance

The rectification mechanism in Py/Pt bilayer ST-FMR experiments is a mixing of the oscillating anisotropic magnetoresistance with the microwave current in the bilayer. The in-plane dependence of AMR is well-known to have a $\cos^2(\phi)$ behavior. We show the $\cos^2(\phi)$ angular dependence of our device below in Fig. 8.

C.   Out-of-plane ST-FMR data for the rectangular bar device

We did perform an OOP angular dependent measurement of the shorted square contact pad sample [Fig. 6 (c) and (d)]. However, the presence of multiple FL and DL torques in the in-plane analysis was troublesome so we did not perform a
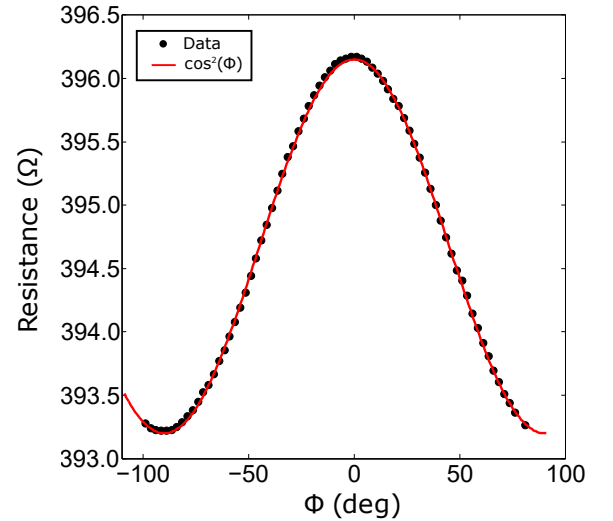

FIG. 8. The in-plane angular behavior of the magnetoresistance is shown above. The ϕ dependence is consistent with the anisotropic magnetoresistance mechanism.

detailed analysis of the OOP dataset. Nevertheless, we show some representative ST-FMR traces here in Fig. 9 (a)-(d) as the field is tipped OOP. The signal to noise was actually better for this sample compared to that of the CPW sample main data, and there was pronounced asymmetry in the ST-FMR signal. We expect that the dynamic non-reciprocity is playing a significant role in this dataset but we chose to focus our study on the CPW sample design structure where we are confident in our understanding of the driving torques.
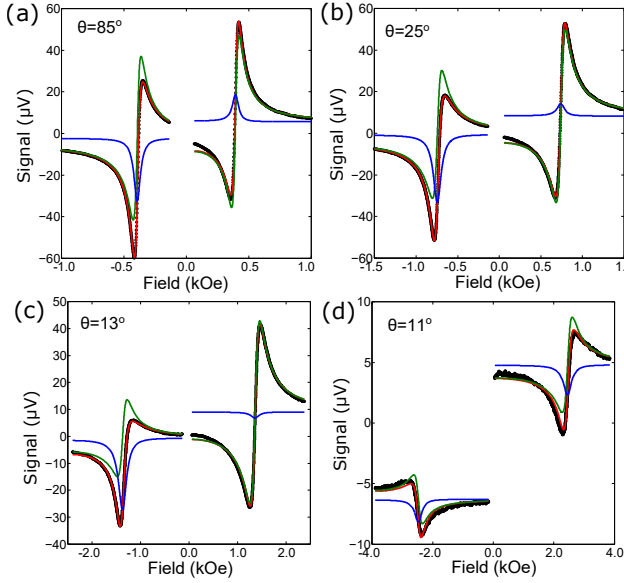
FIG. 9. Here we show some representative ST-FMR traces of the square contact pad device at various values of θ where there is both an in-plane and out-of-plane magnetization. We observe again a clear asymmetry with respect to field reversal that is likely due to dynamic non-reciprocity. Based on the in-plane angular dependence of this device we did not believe that a detailed analysis of the out-of-plane data could be too trustworthy.

D. Conversion to spin Hall angle and lineshape consistency

In the main text we wanted to keep the discussion phenomenologically simple in order to focus on the issue of dynamic non-reciprocity. To this end, our analysis focused on the single fit parameter τ_D/τ_F. Here we mention that if one did performed a lineshape analysis to obtain a spin Hall angle we find a value of our sample that is consistent with the literature. Following Liu[8], the indivdual torques are (in SI units):

$$\tau_D = \frac{\hbar\theta_{SH}J_c}{2e\mu_0 M_{eff}t}, \qquad (9)$$

$$\tau_F = \frac{J_c d}{2}. \qquad (10)$$

Here J_c is the microwave charge current density passing through the bilayer, t is the thickness of the permalloy, d is the thickness of the platinum, and θ_{SH} is the spin Hall angle. In our OOP analysis we find that the the ratio of τ_D/τ_F appears to have some OOP angular dependence. We consider the curve that seems to describe the in-plane values, $\tau_D/\tau_F = 1.5$. Using this value, along with our extraction of M_{eff} obtained from the Kittel analysis in Section A of the Appendix we can solve for θ_{SH}. We estimate that in our sample $\theta_{SH} = 0.07$ (neglecting interface transparency effects etc.[40]).

The estimated value of the spin Hall angle also gives us confidence that a possible phase shift between the Oersted field and the microwave charge current is not influencing our result. As has been pointed out by Harder *et al.*, some device
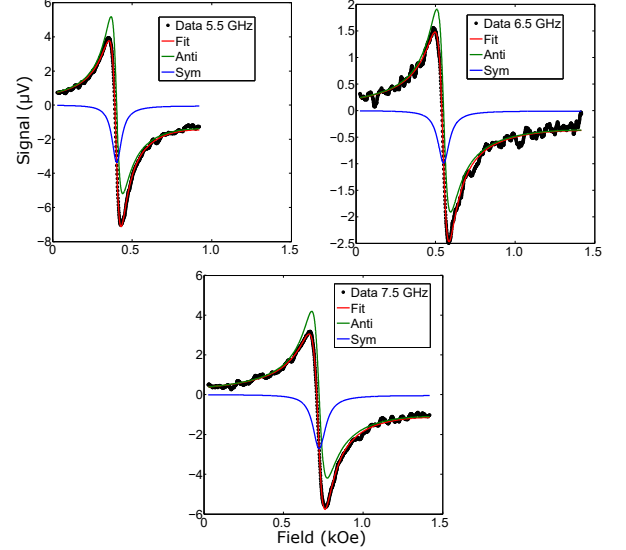

FIG. 10. Frequency dependence of the ST-FMR signal for the coplanar wavguide sample is shown above. The consistent lineshape suggests that no significant phase shift is present.

designs can lead to huge phase shifts in a narrow frequency range[39]. In Fig. 10 we show the lineshape at $\phi = -35°$ for 5.5, 6.5, and 7.5 GHz. The lineshape remains consistent giving us additional confidence that a phase shift is not responsible for our unidirectional lineshapes.

* Present address: Department of Physics, University of Illinois at Urbana-Champaign, Urbana, IL 61801, USA

[1] A. Hoffmann, IEEE Trans. Magn. **49**, 5172 (2013).

[2] J. C. Slonczewski, J. Magn. Magn. Mater. **159**, L1 (1996).

[3] L. Berger, Phys. Rev B **54**, 9353 (1996).

[4] J. C. Slonczewski, J. Magn. Magn. Mater. **195**, L261 (1999).

[5] D. C. Ralph and M. D. Stiles, J. Magn. Magn. Mater. **320**, 1190 (2008).

[6] A. A. Tulapurkar, Y. Suzuki, A. Fukushima, H. Kubota, H. Maehara, K. Tsunekawa, D. D. Djayaprawira, N. Watanabe, and S. Yuasa, Nature **438**, 339 (2005).

[7] J. C. Sankey, P. M. Braganca, A. G. F. Garcia, I. N. Krivorotov, R.

A. Buhrman, and D. C. Ralph, Phys. Rev. Lett. **96**, 227601 (2006).

[8] L. Liu, T. Moriyama, D. C. Ralph and R. A. Buhrman, Phys. Rev. Lett. **106**, 036601 (2011).

[9] J. E. Hirsch, Phys. Rev. Lett. **83**, 1834 (1999).

[10] M. Tsoi, A. G. M. Jansen, J. Bass, W. -C. Chiang, V. Tsoi and P. Wyder, Nature **406**, 46-48 (2000).

[11] J. A. Katine, F. J. Albert, R. A. Buhrman, E. B. Myers, and D. C. Ralph, Phys. Rev. Lett. **84**, 3149 (2000).

[12] L. Liu, C. -F. Pai, Y. Li, H. W. Tseng, D. C. Ralph and R. ABuhrman, Science **336**, 555 (2012).

[13] C. -F. Pai, L. Liu, Y. Li, H. W. Tseng, D. C. Ralph and R. A. Buhrman, Appl. Phys. Lett. **101**, 122404 (2012).

[14] A. R. Mellnik, J. S. Lee, A. Richardella, J. L. Grab, P. J. Mintun, M. H. Fischer, A. Vaezi, A. Manchon, E. -A. Kim, N. Samarth and D. C. Ralph, Nature **511**, 449 (2014).

[15] W. Zhang, M. B. Jungfleisch, F. Freimuth, W. Jiang, J. Sklenar, J. E. Pearson, J. B. Ketterson, Y. Mokrousov and A. Hoffmann, Phys. Rev. B **92**, 144405 (2015).

[16] W. Zhang, J. Sklenar, B. Hsu, W. Jiang, M. B. Jungfleisch, K. Sarkar, F. Y. Fradin, Y. Liu, J. E. Pearson, J. B. Ketterson, Z. Yang and A. Hoffmann. APL Mater. **4**, 032302 (2016).

[17] M. B. Jungfleisch, W. Zhang, J. Sklenar, W. Jiang, J. E. Pearson, J. B. Ketterson and A. Hoffmann, Phys. Rev. B. **93**. 224419 (2016).

[18] T. Chiba, G. E. W. Bauer and S. Takahashi, Phys. Rev. Applied **2**, 034003 (2014).

[19] T. Chiba, M. Schreier, G. E. W. Bauer, and S. Takahashi, J. Appl. Phys. **117**, 17C715 (2015).

[20] M. Schreier, T. Chiba, A. Niedermayr, J. Lotze, H. Huebl, S. Geprägs, S. Takahashi, G. E. W. Bauer, R. Gross and S. T. B. Goennenwein, Phys. Rev. B **92**, 144411 (2015).

[21] J. Sklenar, W. Zhang, M. B. Jungfleisch, W. Jiang, H. Chang, J. E. Pearson, M. Wu, J. B. Ketterson and A. Hoffmann, Phys. Rev. B **92**, 174406 (2015).

[22] M. B. Jungfleisch, W. Zhang, J. Sklenar, J. Ding, W. Jiang, H. Chang, F. Y. Fradin, J. E. Pearson, J. B. Ketterson, V. Novosad, M. Wu and A. Hoffmann, Phys. Rev. Lett. **116**, 057601 (2016).

[23] C. O. Avci, K. Garello, A. Ghosh, M. Gabureac, S. F. Alvarado and P. Gambardella, Nat. Phys. **11**, 570-575 (2015).

[24] H. T. Nembach, J. M. Shaw, M. Weiler, E. Jué and T. J. Silva, Nat. Phys. **11**, 825-829 (2015).

[25] K. Di, V. L. Zhang, H. S. Lim, S. C. Ng, M. H. Kuok, J. Yu, J. Yoon, X. Qiu and H. Yang, Phys. Rev. Lett. **114**, 047201 (2015).

[26] U. H. Pi, K. W. Kim, J. Y. Bae, S. C. Lee, Y. J. Cho, K. S. Kim and S. Seo, App. Phys. Lett. **97**, 162507 (2010).

[27] K. Garello, I. M. Miron, C. O. Avci, F. Freimuth, Y. Mokrousov, S. Blügel, S. Auffret, O. Boulle, G. Gaudin and P. Gambardella, Nat. Nanotech. **8**, 587593 (2013).

[28] C. O. Avci, K. Garello, C. Nistor, S. Godey, B. Ballesteros, A. Mugarza, A. Barla, M. Valvidares, E. Pellegrin, A. Ghosh, I. M. Miron, O. Boulle, S. Auffret, G. Gaudin and P. Gambardella, Phys. Rev. B **89**, 214419 (2014).

[29] X. Qiu, P. Deorani, K. Narayanapillai, K. -S. Lee, K.-J. Lee, H.-W.Lee and H. Yang, Sci. Rep. **4**, 4491 (2014).

[30] A. Hoffmann and S. D. Bader, Phys. Rev. App. **4**, 047001 (2015).

[31] T. R. McGuire amd R. I. Potter, IEEE Trans. Magn. **11**, 1018 (1975).

[32] H. J. Juretschke, J. Appl. Phys. **31**, 1401 (1960).

[33] H. J. Juretschke, J. Appl. Phys. **34**, 1223 (1963).

[34] J. C. Sankey, P. M. Braganca, A. G. F. Garcia, I. N. Krivorotov, R. A. Buhrman and D. C. Ralph, Phys. Rev. Lett. **96**, 227601 (2006).

[35] J. N. Kupferschmidt, S. Adam, and P. W. Brouwer Phys. Rev. B **74**, 134416 (2006).

[36] A. Yamaguchi, H. Miyajima, T. Ono, Y. Suzuki, S. Yuasa, A. Tulapurkar and Y. Nakatani, Appl. Phys. Lett. **90**, 182507 (2007).

[37] Y. S. Gui, N. Mecking, X. Zhou, G. Williams and C. -M. Hu, Phys. Rev. Lett. **98**, 107602 (2007).

[38] N. Mecking, Y. S. Gui and C. -M. Hu, Phys. Rev. B **76**, 224430 (2007).

[39] M. Harder, Z. X. Cao, Y. S. Gui, X. L. Fan, and C.-M. Hu Phys. Rev. B **84**, 054423 (2011).

[40] W. Zhang, E. Han, X. Jiang, S. -H. Yang, and S. S. P. Parkin, Nat. Phys. **11**, 496 (2015).

[41] T. Skinner,"Electrical control of spin dynamics in spin-orbit coupled ferromagnets", Ph.D. thesis, University of Cambridge, 2014.

[42] J. Sklenar, W. Zhang, M. B. Jungfleisch, W. Jiang, H. Saglam, J. E. Pearson, J. B. Ketterson, and A. Hoffmann, AIP Advances **6**, 055603 (2016).